Journal of Materials Chemistry B

Er3+-doped YbPO4 Up-conversion Porous Nanospheres for UCL/CT Bimodal Imaging In Vivo and Chemotherapy

Journal:	*Journal of Materials Chemistry B*
Manuscript ID:	TB-ART-05-2014-000880.R2
Article Type:	Paper
Date Submitted by the Author:	31-Jul-2014

Complete List of Authors:	Zheng, Xiaopeng; Institute of High Energy Physics, Chinese Academy of Sciences, Zhou, Liangjun; University of Chinese Academy of Sciences, College of Materials Science and Opto-Electronic Technology; Chinese Academy of Sciences, Institute of High Energy Physics Bu, Yang; University of Chinese Academy of Sciences, College of Materials Science and Opto-Electronic Technology Yin, Wenyan; Institute of high energy physics, Key Laboratory for Biomedical Effects of Nanomaterials and Nanosafety Hu, Zhongbo; University of Chinese Academy of Sciences, College of Materials Science and Opto-Electronic Technology Li, Meng; Institute of high energy physics, Key Laboratory for Biomedical Effects of Nanomaterials and Nanosafety Gu, Zhanjun; Institute of high energy physics, Zhao, Yuliang; Institute of High Energy Physics, Chinese Academy of Sciences, CAS Key Lab for Biomedical Effects of Nanomaterials and Nanosafety, CAS Key Laboratory of Nuclear Analytical Techniques

Er^{3+}-doped $YbPO_4$ Up-conversion Porous Nanospheres for UCL/CT Bimodal Imaging *In Vivo* and Chemotherapy

Xiaopeng Zheng[a,c], Liangjun Zhou[a,c,d]*,Yang Bu[c], Wenyan Yin[a], Zhongbo Hu[c], Meng Li[a], Zhanjun Gu[a,]*, Yuliang Zhao[a,b]*

[a] Key Laboratory for Biomedical Effects of Nanomaterials and Nanosafety, Institute of High Energy Physics, Chinese Academy of Sciences, Beijing, 100049, P. R. China

[b] Key Laboratory for Biomedical Effects of Nanomaterials and Nanosafety, National Center for Nanoscience and Technology of China, Beijing, 100190, P. R. China

[c] College of Materials Science and Opto-Electronic Technology, University of Chinese Academy of Sciences, Beijing, 100049, P. R. China

[d] College of Aerospace and Materials Engineering, National University of Defense Technology, Changsha, 410073, P. R. China

*Corresponding Authors: zhoulj@ihep.ac.cn, zjgu@ihep.ac.cn, zhaoyuliang@ihep.ac.cn

ABSTRACT

The marriage between nanotechnology and medical technologies holds great promise for the development and improvement of various theranostic media. Here, based on a facile hydrothermal method, polyethyleneimine (PEI) functionalized $YbPO_4$:Er up-conversion porous nanospheres (UCPSs) were fabricated, which combined the capabilities of up-conversion luminescence (UCL)/X-ray computed tomography (CT) bimodal imaging and drug delivery. The resulting hydrophilic PEI functionalized $YbPO_4$:Er UCPSs (PEI-UCPSs) showed uniform morphology and high crystallinity. Moreover, PEI-UCPSs possessed high drug loading capacity, owing to their large specific surface area, which was confirmed by the Brunauer-Emmett-Teller (BET) experiment. The cellular experiments indicated that the PEI-UCPSs had low cytotoxicity and confirmed the performance of the pH-mediated cancer targeting of PEI-UCPSs@DOX. Importantly, due to the ideal UCL property and high CT contrast both *in vitro* and *in vivo*, $YbPO_4$:Er PEI-UCPSs could be used as optical probe and contrast agent for optical imaging and CT imaging, forming a promising platform for simultaneous bioimaging and drug delivery.

Keywords: luminescence, hydrothermal method, porous spheres, bimodality biomedical imaging, chemotherapy

1. Introduction

Much attention have been paid to multifunctional theranostic platform, which could simultaneously act as both therapy method and imaging tool.[1-4] Because of cavity structure for the controlled storage/delivery of therapeutic drugs, porous structured nanomaterials hold great promise for the development and improvement of various theranostic systems.[5-12] Owing to the ideal chemical and optical features, including weak autofluorescence background, near infrared (NIR) excitation with deep penetration, resistance to photobleaching, and biocompatibility, up-conversion nanoparticles (UCNPs) are regarded as a potential alternative to conventional imaging cargos.[13, 14] To combine the properties of UCNPs and porous structured nanomaterials, porous structured UCNPs have been designed.[7] These luminescent porous structured materials not only fulfill the purpose of drug delivery, but also achieve the objective of biological imaging. However, the limited spatial resolution and the absence of 3D tissue details are the key problems, which greatly hamper the development of up-conversion luminescence (UCL) imaging.[15] Fortunately, X-ray computed tomography (CT) is a noninvasive clinical diagnostic tool, with high spatial resolution and 3D visual reconstruction ability.[16] Thus, the bimodal imaging, associating UCL imaging with CT imaging, can overcome the shortcomings and incorporate the advantages of the two imaging methods. As a rule, materials possessing high atomic numbers (Z) tend to absorb X-rays better. Hence, Yb element (Z=70) has higher X-ray absorbance than that of I element (Z=53) in the commercial iopromide CT contrast agent (iopromide).[17] More importantly, owing to the attenuation characteristics of Yb-based nanoparticles (NPs), which are matched with the X-ray photon energy used in clinical applications, they can offer a much higher contrast efficacy than clinical iodinated agents at 120 kVp. Therefore, Yb-based UCNPs have been developed as a promising CT contrast agents and UCL imaging probes.[16, 18] For example, Yb_2O_3[19] and $NaYbF_4$[18, 20] UCNPs have been used for both CT imaging and UCL imaging with good performance. Moreover, $YbPO_4$ is known to be an efficient host lattice of up-conversion (UC) phosphors.[21] Hence, it is promising to develop a theranostic

platform based on the small and hydrophilic $YbPO_4$ up-conversion porous nanospheres (UCPSs), realizing simultaneous UCL/CT bimodal imaging and drug delivery, on which few work have been reported. Additionally, the widely used template-assisted strategy for the UCPSs possesses many drawbacks, including complicated synthetic procedures, poor water-solubility, which hamper the further application of as-obtained porous UC nanomaterials. [22-25] Accordingly, it urgently need to develop template-free processes for porous-structured UC nanomaterials, which can overcome these above drawbacks.[5, 24] The porous nanospheres, prepared by template-free process, are usually hydrophilic and suitable for further applications in the biological field.

Herein, as illustrated in Scheme 1, we developed a multifunctional nano-theranostic platform with small and hydrophilic $YbPO_4$:Er UCPSs, realizing simultaneous UCL/CT bimodal imaging *in vivo* and drug delivery. A facile template-free hydrothermal method was adopted to synthesize polyethyleneimine (PEI) functionalized $YbPO_4$:Er UCPSs (PEI-UCPSs) with uniform morphology, high crystallinity, and porous structure for drug loading. Furthermore, both normal (16HBE) and cancer (A549) cells were employed to investigate cancer cell-killing ability of the PEI-UCPSs@DOX. Importantly, in order to confirm the properties of optical probe and contrast agent for optical imaging and CT imaging, UCL/CT imaging *in vitro* and *in vivo* of the PEI-UCPSs were studied.

2. Experimental Section

Materials

Polyethylenimine (PEI, M.w. = 25000) was purchased from Sigma-Aldrich. $CO(NH_2)_2$ (AR), $NH_4H_2PO_4$ (AR), glycerin (99%), $Yb(NO_3)_3{\cdot}xH_2O$ (x≈5, 99.99 %), $Er(NO_3)_3{\cdot}xH_2O$ (x≈5, 99.9 %) were all supplied by Alfa Aesar Reagent Company. NaOH, HCl, NaCl, Ethanol were supplied by Beijing Chemical Reagent Company. Doxorubicin hydrochloride (DOX, 99.9%) was purchased from Beijing Hua Feng United Technology CO., Ltd. Cell counting kit-8 (CCK-8), Calcein-AM (CA) ,and propidium iodide (PI) were provided by Dojindo Laboratories in Japan. Hoechst 33258 and antifade mounting medium were bought from Beyotime Institute of

Biotechnology. All of the chemicals were analytical grade and used without further purification. Deionized water was used throughout experiments.

2.1 Preparation of Yb Carbonate precursors.

The Yb carbonate precursors were prepared according to an urea-based homogeneous precipitation process.[26] In a typical process, urea ($CO(NH_2)_2$, 0.1 g), yttrbium nitrate (0.1 M, 4.9 mL), erbium nitrate (0.5 M, 0.02 mL), and glycerin (2 mL) were mixed in a Teflon-lined autoclave under thorough stirring at room temperature. After 0.5 h, the colloidal solution was transferred, sealed and heated at 160 °C for 8 h. The products were collected by centrifugation, washing and then dried in lyophilizer.

2.2 Preparation of PEI modified monodisperse $YbPO_4$:Er UCPSs

In a typical procedure, a dispersion containing 28 mg of dried Yb carbonate precursor powder, $NH_4H_2PO_4$ (6 mg), and PEI aqueous solution (1 mg/mL, 16 mL) was added into a Teflon-lined autoclave equipped with a magnetic stir bar. After vigorous stirring at room temperature for 0.5 h, the solution was sealed and heated at 160 °C for 6 h. The products were collected by centrifugation, washing and then dried in lyophilizer.

2.3 Characterization

The morphology and size of the as-synthesized NPs were characterized by the field emission scanning electron microscope (FE-SEM) and transmission electron microscope (TEM, Tecnai G2 20 S-TWIN operated at 200 kV). Powder X-ray diffraction (XRD) patterns of the dried products were measured using a Japan Rigaku D/max-2500 diffractometer with $Cu_{k\alpha}$ radiation (λ=1.5418 Å). The photoluminescence spectrum was obtained by a fluorescence spectrophotometer (Horiba Jobin Yvon FluorolLog3) with an external 980 nm laser. All photos of UCL were acquired by a Nikon D3100 digital camera. CT signals were acquired using a CT system XM-Tracer-130. Fourier Transform infrared (FT-IR) spectra were carried out by a Fourier transform Bruker EQUINOX55 spectrometer with the KBr pellet technique.

2.4 *In vitro* biocompatibility of $YbPO_4$:Er UCPSs

16HBE (a human bronchial epithelial cell line) and A549 (a human lung

adenocarcinoma cell line) cells were employed in this investigation. The cell viabilities of $YbPO_4$:Er PEI-UCPSs with a series of concentration (0, 6.25, 12.5, 25, 50, 100, 200, 400 μg/mL) were studied through the standard CCK-8 assay. The cells were pre-incubated in a 96-well plate (about 2000 cells/well, six wells for each concentration) with six blank-wells for 24 h in a humidified incubator (37 ℃, 5% CO_2). After washing each well with phosphate buffer saline (PBS, 0.01 M, pH = 7.4), PEI-UCPSs of different concentrations were added. Then the cells were continuously incubated in the same condition for 24 h. 100 μL of 10% CCK-8 solution was subsequently added to each well and the plate was kept in the incubator for another 2 h. Finally, the absorbance at 450 nm was measured with a microplate reader (SpectraMax M2, MDC, USA), and the cell viabilities were calculated according to the control groups. Furthermore, inverted fluorescence microscopy (IX73, Olympus, Japan) was used to observed all kinds of cells, which were co-incubated with $YbPO_4$:Er UCPSs (200 μg/mL) for 24 h and then stained by CA and PI via the standard protocol.

2.5 Drug loading and release

The widely applied clinical cancer chemotherapy drug, doxorubicin (DOX), is selected as a model drug to evaluate the loading and release behaviors of the $YbPO_4$:Er PEI-UCPSs@DOX. In detail, drug loading experiment was performed by dispersing 20 mg of PEI-UCPSs in 4 mL of PBS (pH=7.4) containing different concentrations of DOX (50-3000 μM) and continuously stirring for 24 h in dark at room temperature. The supernatant was collected by centrifugation. The DOX loading amount was calculated by the absorbance change of the characteristic absorption peak of DOX solution according to the calibration curve of DOX.

To measure drug release property, the corresponding materials, dispersed in PBS (pH 7.4 or 5.0), were continuously shook at 37 ℃. At certain time intervals, 4 mL of dispersion was taken out for determining the release efficiency by the UV-Vis absorption of supernatant, and then the dispersion was put into original mixture. The released DOX amount was calculated as the same way mentioned above.

2.6 *In Vitro* Drug Delivery Study

16HBE and A549 cells were both employed in the study. In order to make sure the killing cancer cells effect, cytotoxicity of PEI-UCPSs@DOX was investigated via the CCK-8 assay after 24 h co-incubation with different concentrations of PEI-UCPSs@DOX (0, 6.23, 12.5, 25, 50, 100, and 200 μg/mL). Furthermore, after 24 h co-incubation with $YbPO_4$:Er UCPSs@DOX (100 μg/mL), cells were stained with hoechst 33258 via the standard protocol and then observed by using inverted fluorescence microscopy (IX73, Olympus, Japan).

Moreover, DOX molecules with red auto-fluorescence under UV light could also be used as a bio-probe to examine the accumulation and distribution of the released DOX from PEI-UCPSs@DOX in 16HBE and A549 cells. The cells were seeded in a culture plate and grown for 24 h and then were incubated with PEI-UCPSs@DOX (100 μg/mL) at 37 °C for 1 h. Thereafter, the cells were rinsed with PBS for three times to remove free PEI-UCPSs@DOX. Finally, 1 mL of PBS solution was added and the cells were also imaged under inverted fluorescence microscope.

2.7 *In vitro* CT imaging and UCL imaging.

In vitro CT imaging was studied as follows. 1 mL of $YbPO_4$:Er PEI-UCPSs with different concentrations (0, 10, 25, 50 and 100 mM of Yb^{3+}, which was measured to be ~60.9% in PEI-UCPSs by ICP-MS) were dispersed in 0.5% agarose gel solution and placed in 1.5 mL centrifuge tubes for phantom test. CT images were acquired using the CT system XM-Tracer-130. Imaging parameters were as follows: effective pixel size, 80 μm; 70 kV, 100 μA; field of view, 1024 pixels × 1024 pixels. Images of phantom CT images and Hounsfield units (HU) values were analyzed by Osiris software.[4]

In vitro UCL imaging was studied as follows. The A549 cells were put into quartz-bottom dishes, and pre-incubated for 24 h. Cells were washed with PBS (pH = 7.4) and then co-incubated with $YbPO_4$:Er PEI-UCPSs dispersed in DMEM for another 2 h. Finally, all the solution was moved out while 20 μL of antifade mounting medium (Beyotime) was added to prevent hoechst from quenching. After being washed with PBS for three times, cells were stained through co-incubation with hoechst 33258 (Beyotime) for no more than 10 min. Afterwards, the inverted

fluorescence microscope (Olympus IX73) was used to observe the cells under the irradiation of 980 nm laser and UV light.

2.8 Tumor model.

Balb/c nude mice were obtained from Vital River Laboratories and used under protocols approved by Key Laboratory for Biomedical Effects of Nanomaterials and Nanosafety (Institute of High Energy Physics, CAS). The A549 tumors were generated by subcutaneous injection of 2×10^6 cells in 50 μL serum-free DMEM medium onto the hind leg of each female Balb/c nude mice. The mice bearing tumor were used for *in vivo* CT imaging, when the tumor grew up to a diameter of 1 cm.

2.9 *In vivo* CT imaging and UCL imaging.

In vivo CT imaging was performed on SIEMENS Inveon MM Gantry LG CT. In detail, tumor-bearing BALB/C nude mice were intratumorally injected (i. t.) or intravenously (i. v.) injected with $YbPO_4$:Er PEI-UCPSs prior to imaging. After 4 h, tumor-bearing mice were imaged by a small animal X-ray CT (SIEMENS Inveon MM Gantry LG CT). The mice whole body 360° scan lasted about 20 min.

In vivo imaging was carried out in a FluorChem HD2 system equipped with shortpass filter (cut-off wavelength: 800 nm; Thorlabs, Inc). BALB/c mouse was anesthetized by injecting pentobarbital sodium (1% aqueous solution, 100 μL). And then, the mouse was injected subcutaneously with 50 μL of 3 mg/mL PEI-UCPSs at the back. The depth was measured to be 8 mm by needle penetration. The white-light images and luminescence images were captured individually. At the end of the experiments, the animals were disposed according to standard protocol approved by the Key Laboratory for Biomedical Effects of Nanomaterials and Nanosafety (Institute of High Energy Physics, CAS).

3. Results and discussion

3.1 The Synthesis of $YbPO_4$:Er PEI-UCPSs and Characterization

Firstly, the Yb carbonate precursors were synthesized through urea-based hydrothermal method, which was reported in our previous research. As can be seen in the SEM image (Fig. S1), the Yb carbonate are spheres with uniform size of ca. 100 nm. In the next experiment, $YbPO_4$:Er PEI-UCPSs were obtained via a template-free

hydrothermal process using PEI as the surfactant. The SEM image of the PEI-UCPSs (Fig. 1a) indicates that the nanospheres have good uniformity in the size of 100±10 nm and have distinct punctations on its surface (the inset of Fig.1a), confirming the formation of porous structured $YbPO_4$:Er nanospheres. XRD analysis has been conducted to investigate the crystallinity and purity of the as-prepared UCPSs. The XRD pattern (Fig. 1b) shows that the strong and narrow peaks are all in good agreement with the tetragonal phase $YbPO_4$ (JCPDS No.45-0530), indicating the good crystallinity of the as-prepared sample. Additionally, there are no characteristic peaks from other impurities, demonstrating the high purity of the as-prepared nanospheres. To analyze the element component of $YbPO_4$:Er PEI-UCPSs, the EDS analysis has been carried out by scanning in large area on the UCPSs and the EDS spectrum is showed in Fig. 1c. It is found that the peaks correspond to the elements in PEI-UCPSs. Moreover, the successfully functionalized $YbPO_4$:Er UCPSs with PEI polymer is confirmed by the FT-IR spectroscopy as shown in Fig.S2a. These two peaks centered at 1649 and 1405 cm^{-1} are ascribed to internal vibrations of the amide group, demonstrating the successful PEI functionalization on UCPSs.[5, 27] Meanwhile, owing to the functionalizing of the UCPSs with hydrophilic PEI polymer, these nanospheres could be readily dispersed in DI water, forming nearly transparent aqueous solution (Fig. S2b). For the investigation of specific surface area and porous nature of the as-prepared PEI-UCPSs, Brunauer-Emmett-Teller (BET) gas-sorption measurement has been conducted. In Fig. 1d, the N_2 adsorption/desorption isotherms present typical IV-typed isotherms and H1-hysteresis loops.[28, 29] The BET surface area is measured to be about 90.4 m^2/g and the pore volume is 0.482 cm^3/g calculated from N_2 isotherms. The pore size distribution (the inset of Fig. 1d) is calculated using the Barrett-Joyner-Halenda (BJH) distribution from the adsorption branch, indicating the pore-size distributions across the mesoporous (2~50 nm) and macroporous (>50 nm) regions with a maximum peak pore diameter of ca. 22 nm attributed to the large porous structure. The Kirkendall effect, a classical phenomenon in metallurgy, has been considered to be a methodology for such porous inorganic materials. This effect is mainly a non-reciprocal interdiffusion process via the interface of two metals.

Hence, vacancy diffusion appears for compensating the non-equality of the material flow, resulting in the movement of the initial interface. The idea is that, during the reaction, the target product shell forms around the surface of the precursor and takes the shape of the precursor.[24, 30, 31] In our study, accompanying with the hydrothermal-induced decomposition of Yb carbonate precursor nanospheres, $YbPO_4$ punctate forms around the surface of precursor nanospheres, exhibiting rather rougher surfaces and porous structures.

3.2 Cytotoxicity Study of $YbPO_4$:Er UCPSs

We next studied the cytotoxicity of these $YbPO_4$:Er PEI-UCPSs for further applications in bio-field. To evaluate the *in vitro* biocompatibility of the PEI-UCPSs, the CCK-8 assay was carried out to determine the cell viabilities after 24 h co-incubation. And, the results are illustrated in Fig.2a and c. It is clearly observed that the viabilities of both two cells co-incubated with PEI-UCPSs of varied concentrations (up to 400 μg/mL) for 24 h are above 80%, indicating that the PEI-UCPSs induce no observable toxicity on cells. Moreover, cells were stained by CA and PI (Fig. 2b and d) for further confirming the low cytotoxicity of the PEI-UCPSs. In these images, the red fluorescence represent for the dead cells while the green for the alive ones. As displayed in these fluorescence images, the cells are almost alive with few dead ones, indicating that the low cytotoxicity of the PEI-UCPSs.

3.3 Drug Loading and Release

For therapeutic design, we chose the widely used cancer chemotherapeutic drug Doxorubicin (DOX) to study drug loading and release of PEI-UCPSs with large special surface. The UV-Vis spectra were measured to determine the DOX loading and release amount. In detail, the concentration of DOX in the $YbPO_4$:Er UCPSs@DOX composites was determined by the change of the characteristic absorption peak centered at 480 nm. As displayed in the insets of Fig. 3a, the successful loading of DOX onto the PEI-UCPSs is readily confirmed by an obvious color change from white to red. The DOX loading efficiency of PEI-UCPSs in PBS (pH=7.4) is 13.9% (w/w) (Fig. 3a), arising from the large surface area of these porous

structured nanomaterials. The *in vitro* release of DOX from the PEI-UCPSs@DOX could be controlled by changing pH values. As displayed in Fig. 3b, about 40% of DOX is released from the PEI-UCPSs@DOX after 30 h vibration at pH 5.0, while only 10% of DOX is released at pH 7.4. The possible reason is that the protonation of the amino group in the DOX molecule in acidic conditions can weaken its binding to the PEI-UCPSs surface and accelerate the detachment of DOX from PEI-UCPSs@DOX.[32] This pH-dependent drug release could be exploited for cancer chemotherapy applications since the microenvironment in tumors is more acidic than that in normal tissues.[33, 34]

3.4 *In Vitro* Anti-cancer Effect of PEI-UCPSs@DOX

To test the chemotherapeutic effect of the $YbPO_4$:Er PEI-UCPSs@DOX, the cytotoxicities of PEI-UCPSs@DOX on 16HBE and A549 cells were evaluated *in vitro* via CCK-8 assay and Hoechst staining. Comparing the cell viability of 16HBE cells (Fig. 4a) with that of A549 cells (Fig. 4c) after 24 h incubation of PEI-UCPSs@DOX at different concentrations, it is worthwhile noting that the PEI-UCPSs@DOX has much higher cell-killing ability on A549 than 16HBE. Furthermore, in order to avoid the interference of the red fluorescence of DOX under UV light, Hoechst 33258 was used to stain the cells treated with PEI-UCPSs@DOX (100 μg/mL). Fig.4b and d directly show that PEI-UCPSs@DOX cause more dead cells (the bright blue ones) in A549 cells. This fact may be ascribed to the more acidic microenvironment, which results in the increased release of DOX from PEI-UCPSs@DOX. To prove this hypothesis, the ability of the PEI-UCPSs to transport DOX into cells was examined using the inherent fluorescence of DOX, which was observed by inverted fluorescence microscope. Fig. S3 illustrates the inverted fluorescence images of 16HBE and A549 cells after incubation with PEI-UCPSs@DOX (100 μg/mL) for 1 h. Significant intracellular red fluorescent signals of DOX molecules is recorded from the both cells, confirming that the PEI-UCPSs@DOX composite successfully delivery DOX to cells. Moreover, the intracellular red fluorescent signals of PEI-UCPSs@DOX in A549 cells are greater than that in 16HBE ones, indicating the larger amount of DOX. Therefore, the

as-prepared PEI-UCPSs are promising candidates for pH-mediated cancer targeting drug delivery.

3.5 UCL Property of PEI-UCPSs and UCL Imaging *In Vitro* and *In Vivo*

To exploit the UCL imaging, we examined the UCL spectrum, UCL imaging in both cells and BALB/c mouse. The UCL spectrum of the PEI-UCPSs and the corresponding photograph (inset image) under the irradiation of continuous 980 nm laser are showed in Fig. 5a. The two green bands centered at 521 and 541 nm are attributed to $^4H_{11/2}\rightarrow{}^4I_{15/2}$ and $^4S_{3/2}\rightarrow{}^4I_{15/2}$ transitions of Er^{3+} ions, respectively, whereas the red band peaked at 653 nm is assigned to $^4F_{9/2}\rightarrow{}^4I_{15/2}$ transition.[5, 27] To investigate the UCL cell imaging and confirm cellular uptake process of PEI-UCPSs, the A549 cells were treated with PEI-UCPSs (100 μg/mL) for 2 h. Then the cells were observed under an inverted fluorescence microscope (IX71) equipped with mercury lamp and 980 nm laser. The overlay image is showed in Fig. 5b. The green fluorescence is from the PEI-UCPSs under 980 nm laser irradiation, while the blue fluorescence is from the cell nucleuses that stained by Hoechst 33258. As seen from the image, a lot of green fluorescence is found around or in the cells, with no green fluorescence in the cell nucleuses. The result suggests that the PEI-UCPSs can be internalized into the cells with no ability to enter the cell nucleuses. The obtained image also demonstrates that the as-prepared PEI-UCPSs can be used as a good luminescent probe for cell imaging. In the next experiment, to prove the effectiveness of these PEI-UCPSs for *in vivo* imaging of deep tissues, anaesthetized BALB/c mouse was injected at the back of mouse with 100 μL of PEI-UCPSs dispersion. The depth of injection was measured from needle penetration. As seen from Fig. 5c, the green UCL can be clearly seen at the injection position by eyes and the depth of injection reaches to 8 mm.

3.6 CT Imaging *In Vitro* and *In Vivo*

It is known that such Yb-contained NPs can be used as CT imaging contrast agents, since the Yb ions has high atomic number and strong X-ray attenuation. For *in vitro* CT test, various gradient concentrations of $YbPO_4$:Er PEI-UCPSs dispersed in 0.5% agarose gel solution were used. As shown in Fig. 6a and b, with the increase of

Yb concentration, the enhancement of CT signals and continuous rise of the CT values were clearly observed. It is worth noting that the HU value of PEI-UCPSs are higher than that of a commercial iodine-based contrast agent (iopromide) at the same concentration, indicating that PEI-UCPSs provide higher CT contrast than commercial iodine-based contrast agent. This fact is ascribed to that Yb^{3+} ions are more efficiently in X-ray absorption than iopromide (Yb, 3.88 cm^2/g; I, 1.94 cm^2/g at 100 keV, respectively).[16, 35]

Since the PEI-UCPSs had low cytotoxicity and good performance in CT test *in vitro*, the CT imaging *in vivo* using the PEI-UCPSs as contrast agents were carried out on Balb/c nude mice (female) bearing A549 tumor. After being intratumorally (i. t.) injected (5 mg/mL, 50 μL) or intravenously (i. v.) injected (10 mg/mL, 100 μL) with PEI-UCPSs, the mice were imaged by a small animal X-ray CT (SIEMENS Inveon MM Gantry LG CT) (Fig. 6c and d). As seen from Fig. 6c, strong contrast is clearly observed at the injection site of the tumor in the CT image. Meanwhile, the obviously contrast enhancement is observed in tumor of the mouse i. v. injected with PEI-UCPSs (Fig. 6d). The accumulation of PEI-UCPSs in tumor could be attributed to the enhanced permeability and retention effect (EPR) of NPs. Moreover, the enhanced contrast can be also clearly observed in liver and spleen instead of kidney, indicating the accumulation of PEI-UCPSs in liver and spleen via the uptake of reticuloendothelial systems (RES). It is worth noting that the UCPSs precise spatial-specifically monitor the trace of therapeutic agents *in vivo* by CT imaging, potentially opening avenues in the guidance of therapeutic process and the investigation of pharmacokinetics. Therefore, hydrophilic $YbPO_4$:Er PEI-UCPSs (ca. 100 nm) could be applied as a promising CT imaging contrast agent, compensating for the limited UCL imaging depth.

4. Conclusion

In summary, we successfully developed a multifunctional nano-theranostic platform based on PEI functionalized $YbPO_4$:Er UCPSs (PEI-UCPSs), which combined UCL/CT bimodal imaging and drug delivery. Through a facile template-free hydrothermal method, the small and hydrophilic PEI-UCPSs were

fabricated, possessing uniform morphology, well crystalline, and large surface area. Owing to their large surface area that confirmed by the BET experiment, these PEI-UCPSs showed high drug loading capacity. The cellular experiment demonstrated that the PEI-UCPSs had low cytotoxicity and the good anti-cancer efficiency. Furthermore, ideal UCL property and high X-ray absorption impelled the PEI-UCPSs to have good performance in UCL/CT bimodal imaging *in vitro* and *in vivo*. Therefore, PEI-UCPSs have great potential to be applied as the nano-theranostic platform in the cancer treatment.

Acknowledgements

This work was supported by National Basic Research Programs of China (973 program, No. 2012CB932504, 2011CB933403 and 2012CB934001), and National Natural Science Foundation of China (No. 21177128，21303200 and 21101158).

References

1 Z. Gu, L. Yan, G. Tian, S. Li, Z. Chai and Y. Zhao, *Adv. Mater.*, 2013, **25**, 3758.

2 N. M. Idris, M. K. Gnanasammandhan, J. Zhang, P. C. Ho, R. Mahendran and Y. Zhang, *Nat. Med.*, 2012, **18**, 1580.

3 J. V. Jokerst, T. Lobovkina, R. N. Zare and S. S. Gambhir, *Nanomedicine*, 2011, **6**, 715.

4 S. Jin, L. Zhou, Z. Gu, G. Tian, L. Yan, W. Ren, W. Yin, X. Liu, X. Zhang, Z. Hu and Y. Zhao, *Nanoscale*, 2013, **5**, 11910.

5 D. Yang, X. Kang, P. Ma, Y. Dai, Z. Hou, Z. Cheng, C. Li and J. Lin, *Biomaterials*, 2013, **34**, 1601.

6 W. K. Oh, S. Kim, M. Choi, C. Kim, Y. S. Jeong, B. R. Cho, J. S. Hahn and J. Jang, *ACS Nano*, 2010, **4**, 5301.

7 Z. Xu, P. a. Ma, C. Li, Z. Hou, X. Zhai, S. Huang and J. Lin, *Biomaterials*, 2011, **32**, 4161.

8 Y. Wang, P. Yang, P. a. Ma, F. Qu, S. Gai, N. Niu, F. He and J. Lin, *J. Mater. Chem. B*, 2013, **1**, 2056.

9 C. Wang, L. Cheng and Z. Liu, *Biomaterials*, 2011, **32**, 1110.

10 L. L. Li, P. Wu, K. Hwang and Y. Lu, *J. Am. Chem. Soc.*, 2013, **135**, 2411.

11 L. L. Li, R. Zhang, L. Yin, K. Zheng, W. Qin, P. R. Selvin and Y. Lu, *Angew. Chem. Int. Ed.*, 2012, **51**, 6121.

12 D. J. Naczynski, M. C. Tan, R. E. Riman and P. V. Moghe, *J. Mater. Chem. B*, 2014, **2**, 2958.

13 Z. Zhang, L. Wang, J. Wang, X. Jiang, X. Li, Z. Hu, Y. Ji, X. Wu and C. Chen, *Adv. Mater.*, 2012, **24**, 1349.

14 F. Wang, Y. Han, C. S. Lim, Y. Lu, J. Wang, J. Xu, H. Chen, C. Zhang, M. Hong and X. Liu, *Nature*, 2010, **463**, 1061.

15 L. Cheng, C. Wang, X. Ma, Q. Wang, Y. Cheng, H. Wang, Y. Li and Z. Liu, *Adv. Funct. Mater.*, 2013, **23**, 272.

16 N. Lee, S. H. Choi and T. Hyeon, *Adv. Mater.*, 2013, **25**, 2641.

17 H. Lusic and M. W. Grinstaff, *Chem. Rev.*, 2012, **113**, 1641.

18 H. Xing, W. Bu, Q. Ren, X. Zheng, M. Li, S. Zhang, H. Qu, Z. Wang, Y. Hua, K. Zhao, L. Zhou, W. Peng and J. Shi, *Biomaterials*, 2012, **33**, 5384.

19 Z. Liu, Z. Li, J. Liu, S. Gu, Q. Yuan, J. Ren and X. Qu, *Biomaterials*, 2012, **33**, 6748.

20 G. Chen, J. Shen, T. Y. Ohulchanskyy, N. J. Patel, A. Kutikov, Z. Li, J. Song, R. K. Pandey, H. Agren, P. N. Prasad and G. Han, *ACS Nano*, 2012, **6**, 8280.

21 S. Heer, O. Lehmann, M. Haase and H. U. Gudel, *Angew. Chem. Int. Ed.*, 2003, **42**, 3179.

22 F. Zhang, Y. Shi, X. Sun, D. Zhao and G. D. Stucky, *Chem. Mater.*, 2009, **21**, 5237.

23 L. Zhang, M. Yin, H. You, M. Yang, Y. Song and Y. Huang, *Inorg. Chem.*, 2011, **50**, 10608.

24 Z. H. Xu, Y. Cao, C. X. Li, P. A. Ma, X. F. Zhai, S. S. Huang, X. J. Kang, M. M. Shang, D. M. Yang, Y. L. Dai and J. Lin, *J. Mater. Chem.*, 2011, **21**, 3686.

25 J. Yu, R. Hao, F. Sheng, L. Xu, G. Li and Y. Hou, *Nano Research*, 2012, **5**, 679.

26 L. Zhou, W. Yin, W. Ren, Z. Gu, W. Li, S. Jin, L. Yan, G. Tian, Z. Hu and Y. Zhao, *New J. Chem.*, 2012, **36**, 2599.

27 H. T. Wong, M.-K. Tsang, C. F. Chan, K. L. Wong, B. Fei and J. Hao, *Nanoscale*, 2013, **5**, 3465.

28 J. Y. Lei, L. Z. Wang and J. L. Zhang, *ACS Nano*, 2011, **5**, 3447.

29 Z. Zhang, L. Wang, J. Wang, X. Jiang, X. Li, Z. Hu, Y. Ji, X. Wu and C. Chen, *Adv. Mater.*, 2012, **24**, 1418.

30 Y. Yin, R. M. Rioux, C. K. Erdonmez, S. Hughes, G. A. Somorjai and A. P. Alivisatos, *Science*, 2004, **304**, 711.

31 J. B. Fei, Y. Cui, X. H. Yan, W. Qi, Y. Yang, K. W. Wang, Q. He and J. B. Li, *Adv. Mater.*, 2008,

20, 452.

32 C. X. Zhao, L. Yu and A. P. J. Middelberg, *J. Mater. Chem. B*, 2013, **1**, 4828.

33 Z. Deng, Z. Zhen, X. Hu, S. Wu, Z. Xu and P. K. Chu, *Biomaterials*, 2011, **32**, 4976.

34 E. S. Lee, Z. Gao and Y. H. Bae, *J. Control. Release*, 2008, **132**, 164.

35 T. Xiao, S. Wen, H. Wang, H. Liu, M. Shen, J. Zhao, G. Zhang and X. Shi, *J. Mater. Chem. B*, 2013, **1**, 2773.

Table of Content

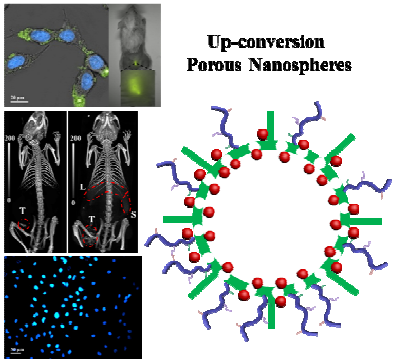

PEI modified up-conversion porous nanospheres were obtained by template-free hydrothermal method, combining up-conversion luminescence/X-ray computed tomography bimodal-imaging with drug delivery.

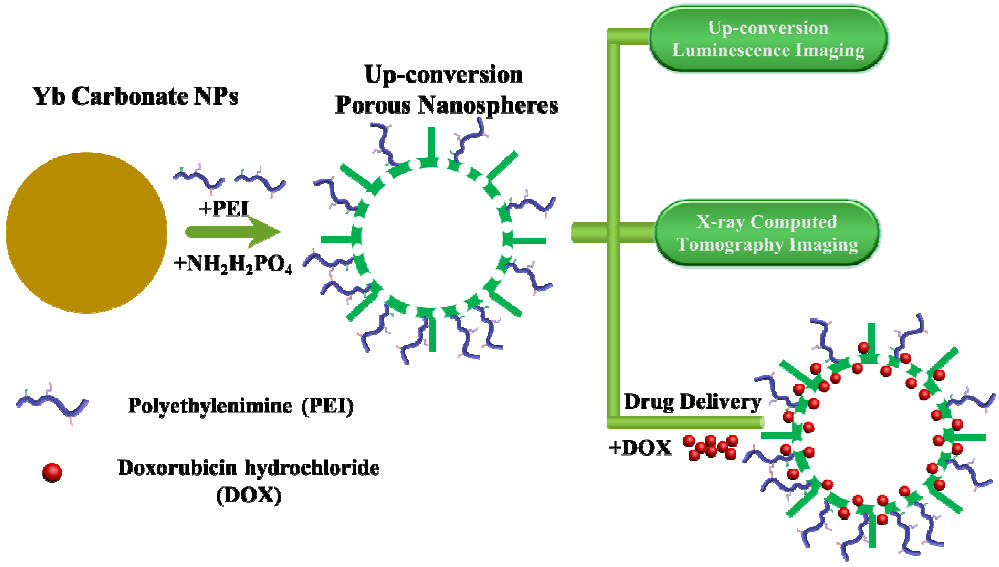

Scheme 1. The scheme of synthesis of up-conversion porous nanospheres for up-conversion luminescence/X-ray computed tomography bimodal imaging and drug delivery.

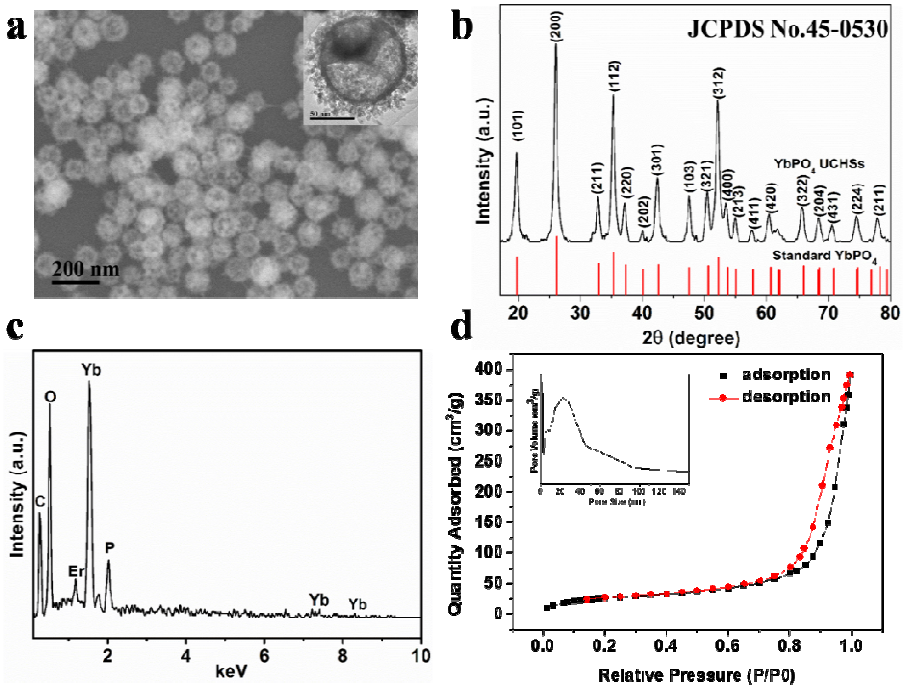

Fig. 1. Characterization of $YbPO_4$:Er UCPSs: (a) SEM image and TEM image (the inset image); (b) XRD pattern; (c) EDX pattern; (d) N_2 adsorption/desorption isotherms and Barrette-Joynere-Halenda (BJH) pore size distribution curves (the inset image) of the $YbPO_4$:Er UCPSs.

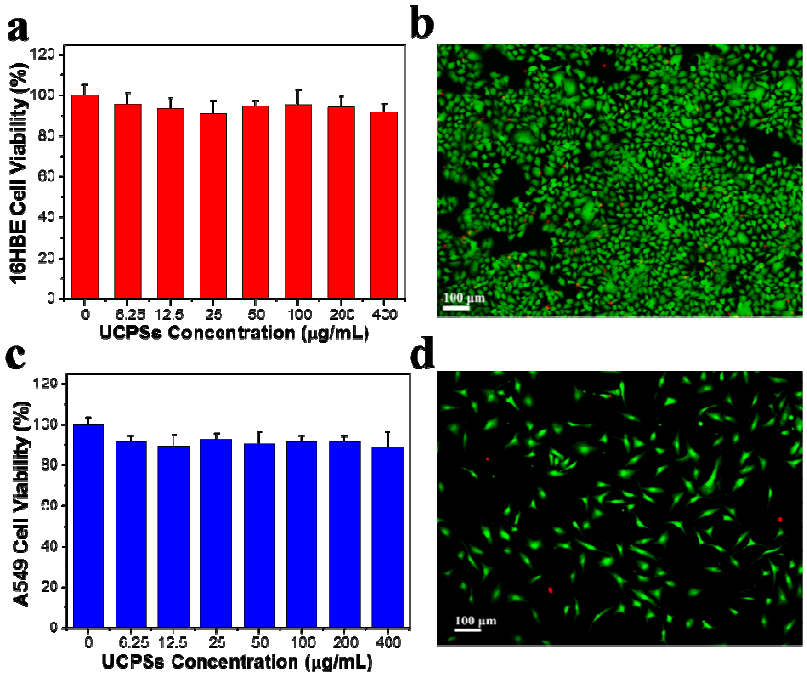

Fig. 2. *In vitro* biocompability study on 16HBE and A549 cells: Cell viabilities of (a) A549 and (c) 16HBE cells incubated for 24 h with PEI-UCPSs at different concentrations; Cell staining studies using Calcein-AM and PI on (b) 16HBE and (d) A549 cells co-incubated with 200 μg/mL for 24 h, respectively.

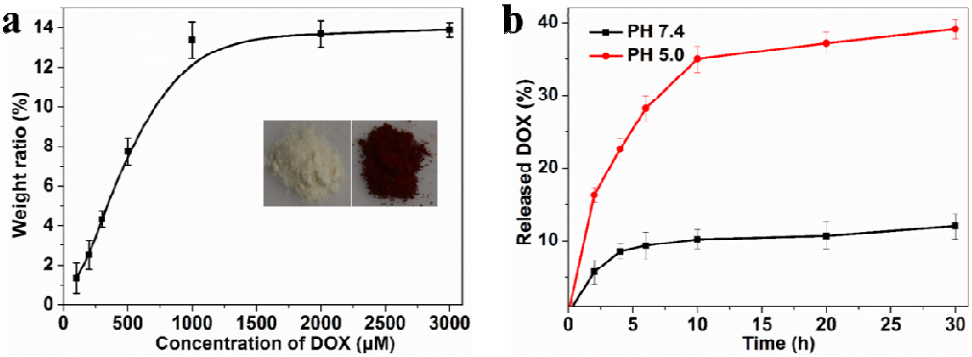

Fig. 3. Drug loading and release behavior study of $YbPO_4$:Er PEI-UCPSs. (a) Quantification of DOX loading at different DOX concentrations in PBS (pH 7.4). Insert: Color change before and after DOX attachment. (b) Real time monitoring DOX release from $YbPO_4$:Er PEI-UCPSs@DOX in PBS at two different pH values.

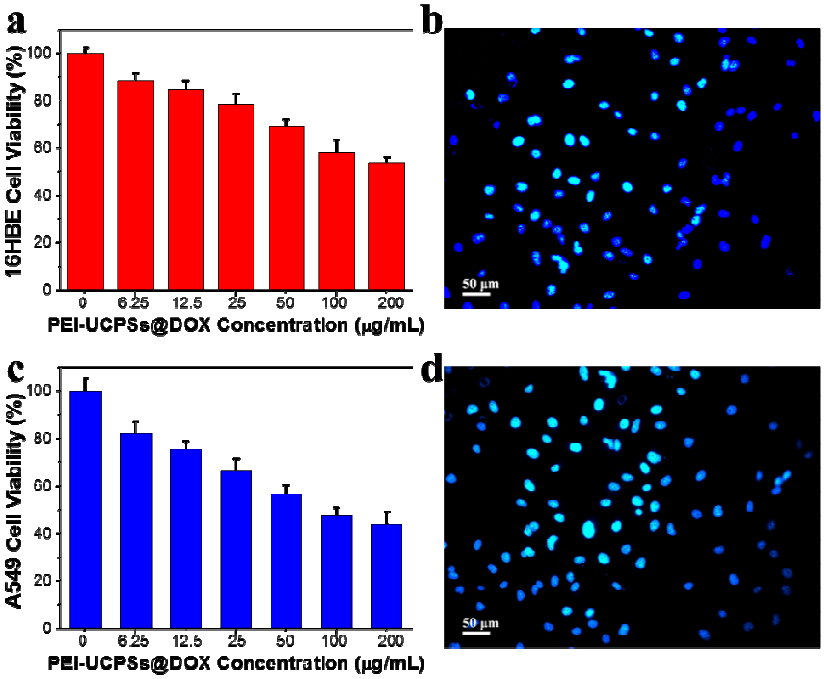

Fig. 4. *In vitro* drug delivery effect and pH-mediated targeting study on 16HBE and A549 cells: cell viability assays at different concentrations of PEI-UCPSs@DOX on (a) 16HBE and (c) A549 cells, respectively; Cell staining studies using hoechst 33258 on (a) 16HBE and (b) A549 cells after 24 h co-incubation with PEI-UCPSs@DOX (100 μg/mL), respectively.

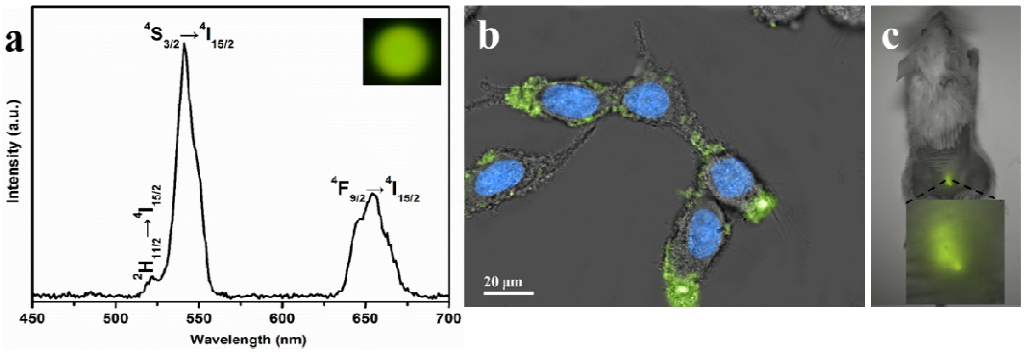

Fig. 5. (a) Room temperature upconversion emission spectrum of the as-obtained $YbPO_4$:Er PEI-UCPSs and the inset: the corresponding luminescent photograph under continuous 980 nm laser excitation. (b) *In vitro* UCL image of A549 cells using the PEI-UCPSs as luminescent probe under excitation with 980 nm laser; (c) *In vivo* UCL animal imaging study by subcutaneously injection at the back of the BALB/c mice with 50 μL of PEI-UCPSs (3 mg/mL) under excitation with 980 nm laser, the depth was ca. 8 mm estimated from needle penetration.

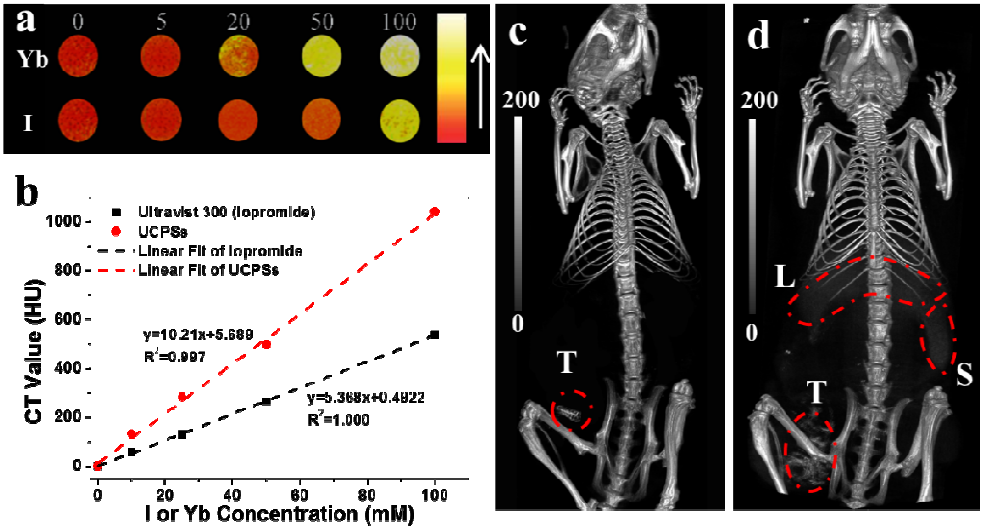

Fig. 6. (a) The colored CT images (the color bar changing from red to white indicates the gradual increase in CT signal intensity) of PEI-UCPSs dispersions (upside) and Ultravist 300 (bottom); (b) The measured HU values of PEI-UCPSs and the clinical CT contrast agent Ultravist 300 as the function of concentrations; (c) CT images of mice after i. t. injection with PEI-UCPSs (5 mg/mL, 50 μL). (d) CT images of mice after i. v. injection with PEI-UCPSs (10 mg/mL, 100 μL). The CT contrast was obviously enhanced in the tumor (T), liver (L) and spleen (S).